

Title	Probing interface defects in top-gated MoS2 transistors with impedance spectroscopy
Authors	Zhao, Peng;Azcatl, Angelica;Gomeniuk, Yuri Y.;Bolshakov, Pavel;Schmidt, Michael;McDonnell, Stephen J.;Hinkle, Christopher L.;Hurley, Paul K.;Wallace, Robert M.;Young, Chadwin D.
Publication date	2017-06-26
Original Citation	Zhao, P., Azcatl, A., Gomeniuk, Y. Y., Bolshakov, P., Schmidt, M., McDonnell, S. J., Hinkle, C. L., Hurley, P. K., Wallace, R. M. and Young, C. D. (2017) 'Probing Interface Defects in Top-Gated MoS2 Transistors with Impedance Spectroscopy', ACS Applied Materials & Interfaces, 9(28), pp. 24348-24356. doi: 10.1021/acsami.7b06204
Type of publication	Article (peer-reviewed)
Link to publisher's version	10.1021/acsami.7b06204
Rights	This document is the Accepted Manuscript version of a Published Work that appeared in final form in ACS Applied Materials & Interfaces, copyright © American Chemical Society after peer review and technical editing by the publisher. To access the final edited and published work see <a href="http://pubs.acs.org/doi/abs/10.1021/acsami.7b06204">http://pubs.acs.org/doi/abs/10.1021/acsami.7b06204</a>
Download date	2024-02-22 04:40:05
Item downloaded from	<a href="https://hdl.handle.net/10468/4682">https://hdl.handle.net/10468/4682</a>



# UCC

**University College Cork, Ireland**  
Coláiste na hOllscoile Corcaigh

## Probing Interface Defects in Top-Gated MoS Transistors with Impedance Spectroscopy

Peng Zhao, Angelica Azcatl, Yuri Y Gomeniuk, Pavel Bolshakov, Michael Schmidt, Stephen J McDonnell, Christopher L Hinkle, Paul K. Hurley, Robert M. Wallace, and Chadwin Young

*ACS Appl. Mater. Interfaces*, **Just Accepted Manuscript** • DOI: 10.1021/acsami.7b06204 • Publication Date (Web): 26 Jun 2017

Downloaded from <http://pubs.acs.org> on July 3, 2017

### Just Accepted

“Just Accepted” manuscripts have been peer-reviewed and accepted for publication. They are posted online prior to technical editing, formatting for publication and author proofing. The American Chemical Society provides “Just Accepted” as a free service to the research community to expedite the dissemination of scientific material as soon as possible after acceptance. “Just Accepted” manuscripts appear in full in PDF format accompanied by an HTML abstract. “Just Accepted” manuscripts have been fully peer reviewed, but should not be considered the official version of record. They are accessible to all readers and citable by the Digital Object Identifier (DOI®). “Just Accepted” is an optional service offered to authors. Therefore, the “Just Accepted” Web site may not include all articles that will be published in the journal. After a manuscript is technically edited and formatted, it will be removed from the “Just Accepted” Web site and published as an ASAP article. Note that technical editing may introduce minor changes to the manuscript text and/or graphics which could affect content, and all legal disclaimers and ethical guidelines that apply to the journal pertain. ACS cannot be held responsible for errors or consequences arising from the use of information contained in these “Just Accepted” manuscripts.

# Probing Interface Defects in Top-Gated MoS<sub>2</sub> Transistors with Impedance Spectroscopy

Peng Zhao,<sup>1</sup> Angelica Azcatl,<sup>1</sup> Yuri Y. Gomeniuk,<sup>2,3</sup> Pavel Bolshakov,<sup>1</sup> Michael Schmidt,<sup>2</sup> Stephen J. McDonnell,<sup>4</sup> Christopher L. Hinkle,<sup>1</sup> Paul K. Hurley,<sup>2</sup> Robert M. Wallace,<sup>1</sup> and Chadwin D. Young<sup>\*,1</sup>

<sup>1</sup>Department of Materials Science and Engineering, The University of Texas at Dallas, 800 W Campbell Rd, Richardson, TX 75080, USA

<sup>2</sup>Tyndall National Institute, Department of Chemistry, University of College Cork, Lee Maltings, Dyke Parade, Cork, Ireland

<sup>3</sup>V. Lashkaryov Institute of Semiconductor Physics, NAS of Ukraine, 41, pr. Nauki, Kyiv, Ukraine

<sup>4</sup>Department of Materials Science and Engineering, The University of Virginia, Charlottesville, VA, USA

**Abstract** The electronic properties of the HfO<sub>2</sub>/MoS<sub>2</sub> interface were investigated using multi-frequency capacitance-voltage (C-V) and current-voltage characterization of top-gated MoS<sub>2</sub> metal-oxide-semiconductor field effect transistors (MOSFETs). The analysis was performed on few layer (5 - 10) MoS<sub>2</sub> MOSFETs fabricated using photolithographic patterning with 13 nm and 8 nm HfO<sub>2</sub> gate oxide layers formed by atomic layer deposition after in-situ UV-O<sub>3</sub> surface functionalization. The impedance response of the HfO<sub>2</sub>/MoS<sub>2</sub> gate stack indicates the existence of specific defects at the interface, which exhibited either a frequency dependent distortion similar to conventional Si MOSFETs with unpassivated silicon dangling bonds, or a frequency dispersion over the entire voltage range corresponding to depletion of the HfO<sub>2</sub>/MoS<sub>2</sub> surface,

1  
2  
3 consistent with interface traps distributed over a range of energy levels. The interface defects  
4 density ( $D_{it}$ ) was extracted from the C-V responses by the high-low frequency and the multiple-  
5 frequency extraction methods, where a  $D_{it}$  peak value of  $1.2 \times 10^{13} \text{ cm}^{-2} \text{ eV}^{-1}$  was extracted for a  
6 device (7-L MoS<sub>2</sub> and 13 nm HfO<sub>2</sub>) exhibiting a behavior approximating to a single trap  
7 response. The MoS<sub>2</sub> MOSFET with 4-L MoS<sub>2</sub> and 8 nm HfO<sub>2</sub> gave  $D_{it}$  values ranging from  
8  $2 \times 10^{11} \text{ cm}^{-2} \text{ eV}^{-1}$  to  $2 \times 10^{13} \text{ cm}^{-2} \text{ eV}^{-1}$  across the energy range corresponding to depletion near the  
9 HfO<sub>2</sub>/MoS<sub>2</sub> interface. The gate current was below  $10^{-7} \text{ A/cm}^2$  across the full bias sweep for both  
10 samples indicating continuous HfO<sub>2</sub> films resulting from the combined UV ozone and HfO<sub>2</sub>  
11 deposition process. The results demonstrated that impedance spectroscopy applied to relatively  
12 simple top-gated transistor test structures provides an approach to investigate electrically active  
13 defects at the HfO<sub>2</sub>/MoS<sub>2</sub> interface and should be applicable to alternative TMD materials,  
14 surface treatments and gate oxides as an interface defect metrology tool in the development of  
15 TMD-based MOSFETs.  
16  
17  
18  
19  
20  
21  
22  
23  
24  
25  
26  
27  
28  
29  
30  
31  
32

33  
34  
35  
36  
37  
38 **Keywords** Molybdenum disulfide (MoS<sub>2</sub>), high-*k* dielectrics, interface defects, electrical  
39 characterization, top-gated transistors, capacitance – voltage (C-V).  
40  
41  
42  
43  
44  
45

## 46 **Introduction**

47  
48  
49 Over the past decade, two-dimensional (2-D) materials have attracted considerable attention  
50 due to their atomically-thin structure and their unique electronic, optical and mechanical  
51 properties<sup>1-3</sup>. Among these materials, transition metal dichalcogenides (TMDs) have  
52 demonstrated satisfactory energy bandgap values and promising properties for future  
53  
54  
55  
56  
57  
58  
59  
60

1  
2  
3 applications in electronics and optoelectronics <sup>4-17</sup>. Molybdenum disulfide (MoS<sub>2</sub>), as the most  
4 explored TMD material, has been reported to exhibit an electron mobility of 55 cm<sup>2</sup>/V·s in a  
5 top-gated transistor with a single layer of MoS<sub>2</sub> <sup>4-6</sup>, and a theoretical value of 410 cm<sup>2</sup>/V·s at  
6 room temperature <sup>7</sup>. Moreover, compared with monolayer MoS<sub>2</sub>, few-layer MoS<sub>2</sub> has been  
7 predicted and experimentally demonstrated as an excellent channel material to achieve high  
8 mobility and reduced contact resistivity <sup>8-12</sup>. With the ultimate electrostatic control due to the 2-  
9 D structure, an energy gap in the range of 1.2eV to 1.8eV, and the high mobility value, MoS<sub>2</sub> is  
10 especially attractive for high performance, low power-consumption flexible electronics <sup>1,10,18,19</sup>.

11  
12  
13  
14  
15  
16  
17  
18  
19  
20  
21  
22  
23 As the utilization of high dielectric constant (high-*k*) gate oxide material in conventional  
24 silicon CMOS processing has been demonstrated to reduce the gate leakage and enable further  
25 scaling of transistors, high-*k* dielectrics are also considered extensively for TMD transistors  
26 <sup>5,10,11,16,18-28</sup>. In addition, high-*k* materials can suppress the coulombic scattering in low  
27 dimensional nanostructures, increasing the carrier mobility, as shown in the literature with both  
28 theoretical simulation <sup>20</sup> and experimental evidence <sup>5,11</sup>. Although back gated structures are ideal  
29 for contact and doping research on TMD transistors <sup>8,29,30</sup>, top gate devices are more attractive  
30 for integrated circuit manufacturing. Thus, investigating high-*k* deposition on TMDs and  
31 understanding the interface properties is an important scientific and technological research area.

32  
33  
34  
35  
36  
37  
38  
39  
40  
41  
42  
43  
44  
45 An obstacle of integrating high-*k* dielectrics on these 2-D materials is the lack of bonds  
46 available at the surface that enables thin film deposition <sup>21,22</sup>. Many top-gated transistors in the  
47 literature adopted thick gate dielectric deposition, usually from 15 nm to 50 nm <sup>5,11,16,23</sup>, to avoid  
48 pin holes and non-uniformity in the dielectric. Recently, multiple surface functionalization  
49 methodologies have been reported for thin, uniform high-*k* dielectric deposition on MoS<sub>2</sub> <sup>22,24-27</sup>.  
50 Metal seed layers <sup>24</sup>, oxygen plasma treatment <sup>22,25</sup> and ultraviolet-ozone (UV-O<sub>3</sub>) treatment <sup>26,27</sup>  
51  
52  
53  
54  
55  
56  
57  
58  
59  
60

1  
2  
3 are promising pre-deposition approaches to gain a uniform dielectric layer. However, since the  
4  
5 ultimate goal of these approaches is the enhancement of electronic device performance, detailed  
6  
7 reports on device performance related to the impacts of these treatments is vital, but only shown  
8  
9 in a few papers<sup>24,25,31</sup>. Our previous research suggested that defects existed at the high-*k*/MoS<sub>2</sub>  
10  
11 interface region after an ex-situ UV-O<sub>3</sub> treatment<sup>28</sup>, but the gate oxide leakage on these large  
12  
13 area MOS structures affected the analysis, due to the rough surface of the bulk MoS<sub>2</sub> sample and  
14  
15 relatively large capacitor area. Recently, Azcatl et al.,<sup>26,27</sup> reported that the non-destructive (i.e.,  
16  
17 no Mo-oxide formation) in-situ UV-O<sub>3</sub> treatment featured a uniform atomic layer deposited  
18  
19 (ALD) high-*k* oxide without unexpected interfacial layers for exfoliated MoS<sub>2</sub>.  
20  
21  
22  
23  
24

25 Impedance measurements are recognized as one of the fastest and most robust methods to  
26  
27 investigate properties of a dielectric and its interface with the underlying substrate. However,  
28  
29 impedance measurements of metal/high-*k* dielectric/TMD MOS system have only been reported  
30  
31 in a limited number of works<sup>10,11,18,31–33</sup>. Most publications report capacitance - voltage (C-V)  
32  
33 curves without further analysis<sup>10,11,32</sup>, or back-gated capacitors with high-*k* deposited on Si<sup>33</sup>.  
34  
35 Recently, S. Park et al.<sup>31</sup> reported C-V characteristics of capacitors with Al<sub>2</sub>O<sub>3</sub> on 100-200 nm  
36  
37 thick MoS<sub>2</sub> yielding  $D_{it}$  values of  $10^{11} \text{ cm}^{-2} \text{ eV}^{-1}$  to  $10^{14} \text{ cm}^{-2} \text{ eV}^{-1}$ . For high-*k* on chemical-vapor-  
38  
39 deposited (CVD) MoS<sub>2</sub> thin films, a comprehensive study of dielectric impedance was  
40  
41 performed, showing  $D_{it}$  extraction and modeling work based on capacitors with 30 nm ALD  
42  
43 HfO<sub>2</sub> on monolayer MoS<sub>2</sub> with 2nm Al as an interfacial seed layer<sup>18</sup>. Another relevant and useful  
44  
45  $D_{it}$  extraction work has been reported by Takenaka et al.<sup>33</sup>, which uses the Terman method to  
46  
47 analyze and compare interfaces of MoS<sub>2</sub> and SiO<sub>2</sub>/HfO<sub>2</sub>/Al<sub>2</sub>O<sub>3</sub>. The extracted  $D_{it}$  values are  
48  
49 about  $1 \times 10^{13} \text{ cm}^{-2} \text{ eV}^{-1}$  regardless of the dielectric selection for back-gated devices on semi-bulk  
50  
51 MoS<sub>2</sub>. However, the device architecture may not be commensurate with the necessary solution  
52  
53  
54  
55  
56  
57  
58  
59  
60

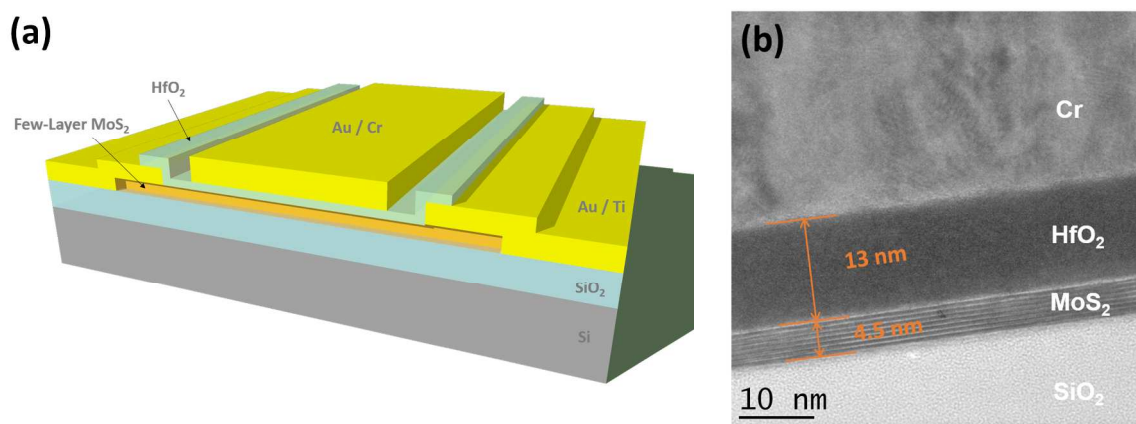
1  
2  
3 for continued device scaling where top-gated architectures dominate. Here, dielectric/substrate  
4 interfaces are dependent upon how device fabrication was executed, and therefore, should be  
5 investigated in this context.  
6  
7  
8  
9

10  
11 In this work, we designed and fabricated top-gated transistors on exfoliated, few-layer MoS<sub>2</sub>  
12 as the test structures, with an in-situ UV-O<sub>3</sub> functionalization<sup>26,27</sup> and 8 to 13 nm ALD HfO<sub>2</sub>,  
13 which are among the thinnest high-*k* dielectrics on top-gate TMD MOSFETs to date. As we use  
14 photolithography for source/drain and gate patterning, the gated area is sufficiently large for C-V  
15 characterization. Both transistor performance and gate-stack interface properties were  
16 characterized, with an emphasis on the impedance spectroscopy of the dielectric. The interface  
17 defect density ( $D_{it}$ ) was extracted and analyzed by three different methods. Besides reporting the  
18 interface properties of our transistors, the methodology can be potentially applied to other TMDs  
19 and surface functionalization, beyond MoS<sub>2</sub> and UV-O<sub>3</sub> treatment.  
20  
21  
22  
23  
24  
25  
26  
27  
28  
29  
30  
31  
32  
33  
34  
35

## 36 **Experimental Methods**

37  
38  
39 The transistor structure used for the few-layer MoS<sub>2</sub> MOSFETs examined in this work is  
40 shown in Fig. 1a. Before device fabrication, 270nm SiO<sub>2</sub> was thermally grown on highly doped  
41 p-type Si wafers as a substrate. Few-layer MoS<sub>2</sub> flakes were mechanically exfoliated from  
42 commercially available natural MoS<sub>2</sub> crystals and transferred onto the SiO<sub>2</sub>. By using  
43 conventional photolithography, we aligned a source/drain pattern on the photomask directly on  
44 the selected flake. After patterning, Au/Ti (380/20nm) was deposited as contacts in an e-beam  
45 evaporator at  $2 \times 10^{-6}$  Torr, followed by a lift-off process. Thereafter, a 15-minute in-situ UV-O<sub>3</sub>  
46 surface treatment<sup>26</sup> was performed. The UV-O<sub>3</sub> is generated based on irradiance from the fused  
47  
48  
49  
50  
51  
52  
53  
54  
55  
56  
57  
58  
59  
60

1  
2  
3 quartz envelope, low pressure UV Hg lamp employed previously<sup>26,27</sup> and is estimated to be 5  
4  
5 mW/cm<sup>2</sup> which ensures no etching or Mo-oxide formation according to S. Park et al.<sup>31</sup>  
6  
7  
8 Following the UV-O<sub>3</sub> surface preparation, HfO<sub>2</sub> was deposited at 200°C in the ALD chamber  
9  
10 immediately after the treatment without a break in vacuum. The thermal ALD used H<sub>2</sub>O and  
11  
12 TDMA-Hf as the precursors, and started the deposition with a TDMA-Hf pulse. We intentionally  
13  
14 avoided annealing the HfO<sub>2</sub> after deposition to study the effects of the UV-O<sub>3</sub> functionalization  
15  
16 treatment and its role on HfO<sub>2</sub>/MoS<sub>2</sub> interface properties without the impact of any subsequent  
17  
18 annealing. The final step of fabrication was patterning and evaporating of Au / Cr (250/50nm)  
19  
20 metal gate. The typical MoS<sub>2</sub> thickness studied in our work was about 5-10 layers (3-6 nm). The  
21  
22 device size was determined by both lithography and the flake shape. Electrical measurements in  
23  
24 this work were performed using a Keithley 4200 Semiconductor Characterization System and an  
25  
26 Agilent E4980A LCR meter at room temperature (25°C) in a shielded probe station.  
27  
28  
29  
30  
31  
32  
33  
34  
35



51  
52  
53  
54  
55  
56  
57  
58  
59  
60

**Figure 1.** (a) Schematic cross section of the top-gated MoS<sub>2</sub> field effect transistor structure used in this work. Gate stack: Au / Cr / HfO<sub>2</sub> / MoS<sub>2</sub>. (b) Cross sectional transmission electron microscopic image of the metal/HfO<sub>2</sub>/MoS<sub>2</sub> transistor gate stack. 13nm HfO<sub>2</sub> is uniformly deposited on a 7-layer MoS<sub>2</sub> flake, showing no evidence of unintentional oxidation of the MoS<sub>2</sub> surface.



## Results and Discussion

A high-resolution transmission electron microscopic (TEM) image is shown in Fig.1b, illustrating the cross section of a device gate stack with 7 layer MoS<sub>2</sub> and a 13 nm HfO<sub>2</sub> dielectric. The active channel length under the metal gate is 6.5 μm and the channel width is 9.5 μm. Fig. 2a shows the I<sub>DS</sub>-V<sub>GS</sub> and the gate leakage characteristics for this MoS<sub>2</sub> transistor. V<sub>DS</sub> was kept at 0.5V. An excellent on/off ratio of 10<sup>6</sup> was observed, with an ultra-low leakage current on the gate. The MoS<sub>2</sub> was intrinsically n-type doped, consistent with our previous observation<sup>28</sup> and literature reports<sup>5,8,24,29</sup>. The relatively large negative threshold voltage (V<sub>T</sub> = -3V) is possibility due to the fixed positive charge in the dielectric layer(s). Similar large |V<sub>T</sub>| was also observed by other researchers using top-gated MoS<sub>2</sub> transistors with high-*k* dielectrics<sup>11,24</sup>. Since the HfO<sub>2</sub> is deposited at low temperature (200 °C) with no post deposition annealing (to assess the UV-O<sub>3</sub> treatment without convolution from additional annealing), a possible net oxide charge being present in the HfO<sub>2</sub> layer may result. Furthermore, possible contribution of induced charges in the underlying SiO<sub>2</sub> from potential x-rays exposure during the electron beam deposition process – which was used to form the metal gate and source/drain regions – could occur. Thus, both oxide layers could possess trapped charge. Assuming the threshold voltage shift ΔV=-3V originates from oxide charges, the density of the positive fixed charges can be estimated by  $Q_f / q = - C_{ox} \cdot \Delta V / q = 1.4 \times 10^{13} / \text{cm}^2$ . Fig. 2b shows the I<sub>DS</sub>-V<sub>DS</sub> curves with V<sub>GS</sub> swept from -4 V to 0 V. A non-linear region was observed at low V<sub>DS</sub>, likely because of high resistance Schottky barriers at the source/drain contacts associated with this unannealed device<sup>5,34</sup>. This is expected, as there is no intentional doping in the MoS<sub>2</sub> film in the source and drain region. As is the case in conventional 3D semiconductors, increasing the doping

in the MoS<sub>2</sub> film to high concentrations ( $> 1 \times 10^{19} \text{ cm}^{-3}$ ), for example via Nb doping<sup>35</sup>, significantly reduces the specific contact resistivity at the Ti/MoS<sub>2</sub> interface. In addition, it is noted from Fig.1a that the top-gated MOSFET has non-gated regions between the gate edge and the source and drain contacts (approximately 1-2 $\mu\text{m}$  on each side), which is another source of series resistance in the structure.

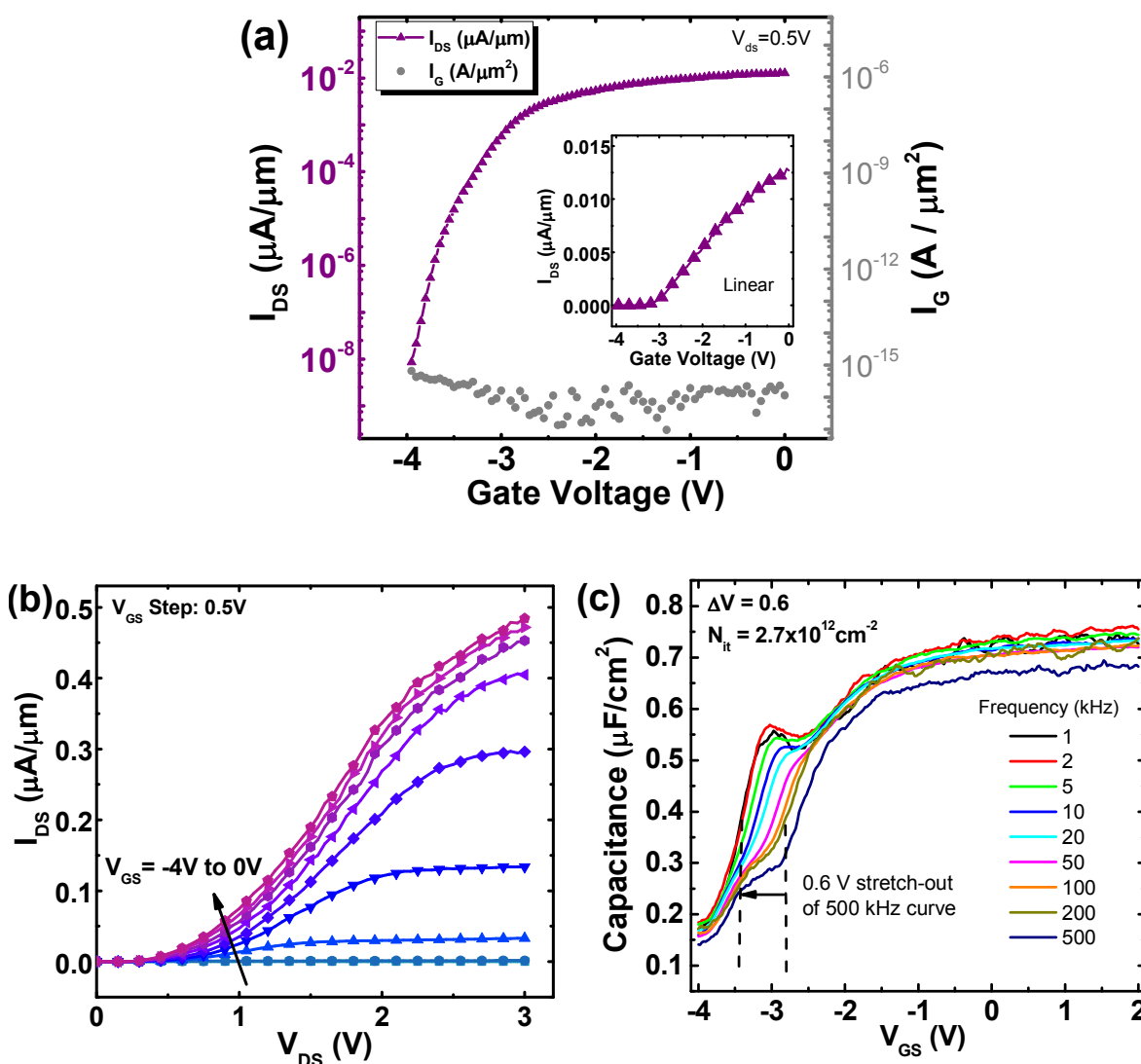
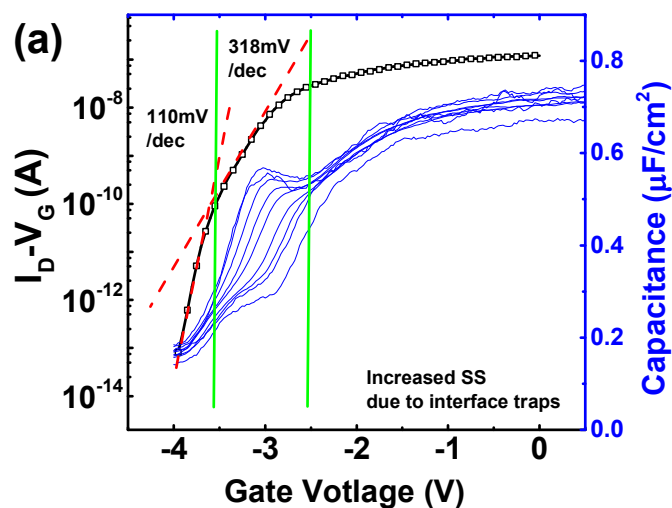
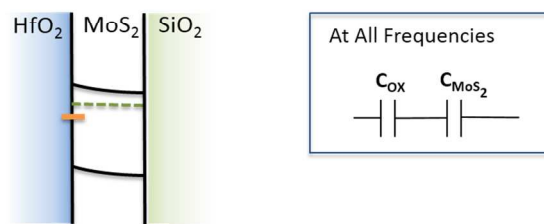


**Figure 2.** Electrical characterization of device with 13 nm HfO<sub>2</sub> and 7-layer MoS<sub>2</sub> (L=6.5 $\mu\text{m}$ , W=9.5 $\mu\text{m}$ ). (a)  $I_{DS}$  -  $V_{GS}$ :  $I_{ON}/I_{OFF} = 10^6$  with ultra-low gate leakage; (b)  $I_{DS}$  -  $V_{DS}$  with  $V_{GS}$  from -4 V to 0 V; (c) C-V: frequency

dependence, where a “hump” in the range -2.5 to -3.5 V is indicating an interface defect response. The 0.6 V stretch-out of 500 kHz curve indicates the Fermi energy pinning at MoS<sub>2</sub> / HfO<sub>2</sub> interface.



(b) (i)  $V_{GS} > -2.8$  V in depletion region



(ii)  $-3.4$  V  $< V_{GS} < -2.8$  V ( $E_F$  pinned)

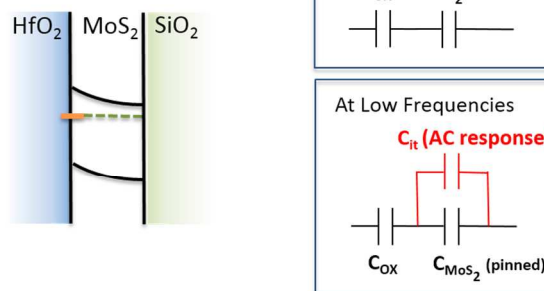


**Figure 3.** (a)  $I_D$ - $V_G$  and multi-frequency C-V overlaid to illustrate the impact of  $D_{it}$  in both measurements occurs at the same  $V_g$ . SS is degraded due to interface traps and  $D_{it} = 1.6 \times 10^{13} \text{ cm}^{-2} \text{ eV}^{-1}$  is estimated. (b) Energy band diagram of high- $k$  / MoS<sub>2</sub> interface and equivalent circuits. (i) At gate voltages higher than -2.8 V or lower than -3.4

1  
2  
3 V, the total AC capacitance is due to the  $C_{ox}$  and  $C_{MoS_2}$  connected in series. (ii) At gate voltage between -3.4 V and -  
4  
5 2.8 V, the  $E_F$  is pinned at interface, and there is an AC response at low frequencies due to  $D_{it}$  but no AC response at  
6  
7 high frequencies.  
8

9  
10 To investigate the electronic properties at  $HfO_2/MoS_2$  interface, the source and drain were  
11  
12 connected to one terminal of the LCR meter, while the gate is connected to the other terminal.  
13  
14 Variable frequency C-V measurements were conducted. The back gate contact was intentionally  
15  
16 floated to minimize the effect from oxide charge in the underlying  $SiO_2$ . The frequency  
17  
18 dependence is shown in Fig. 2c. Since this transistor operates in accumulation mode, the reaction  
19  
20 of the majority carriers (electrons) to the ac signal is observed. In contrast to our previous study  
21  
22 on the ex-situ UV- $O_3$  treatment and bulk  $MoS_2$  crystals<sup>28</sup>, these C-V frequency dependence  
23  
24 results showed a highly improved high- $k/MoS_2$  interface, with significantly less dispersion and  
25  
26 lower gate leakage due to the in-situ UV- $O_3$  treatment and the few-layer TMD thickness. The C-  
27  
28 V characteristics demonstrate an approximately constant capacitance for positive gate voltage,  
29  
30 corresponding to the  $HfO_2$  gate oxide capacitance, and a decrease in capacitance in the region -  
31  
32 2V to -4 V, consistent with depletion of negative charge at the  $HfO_2/MoS_2$  interface. It is noted  
33  
34 that the region of surface depletion in the C-V response in Fig. 2c, is consistent with the sub-  
35  
36 threshold region in the transfer characteristics in Fig. 2a. The measured accumulation  
37  
38 capacitance is  $0.76\mu F/cm^2$ . Based on cross section TEM images, the  $HfO_2$  is 13nm, and assuming  
39  
40 a  $k$  value of 17 for ALD grown  $HfO_2$ , this would yield a maximum capacitance value of  
41  
42  $1.1\mu F/cm^2$ . The lower value obtained experimentally, suggests the possibility of a lower  $k$  value  
43  
44 interface transition region between the  $HfO_2$  and the  $MoS_2$  which is not immediately obvious  
45  
46 from the TEM analysis.  
47  
48  
49  
50  
51  
52  
53  
54  
55  
56  
57  
58  
59  
60

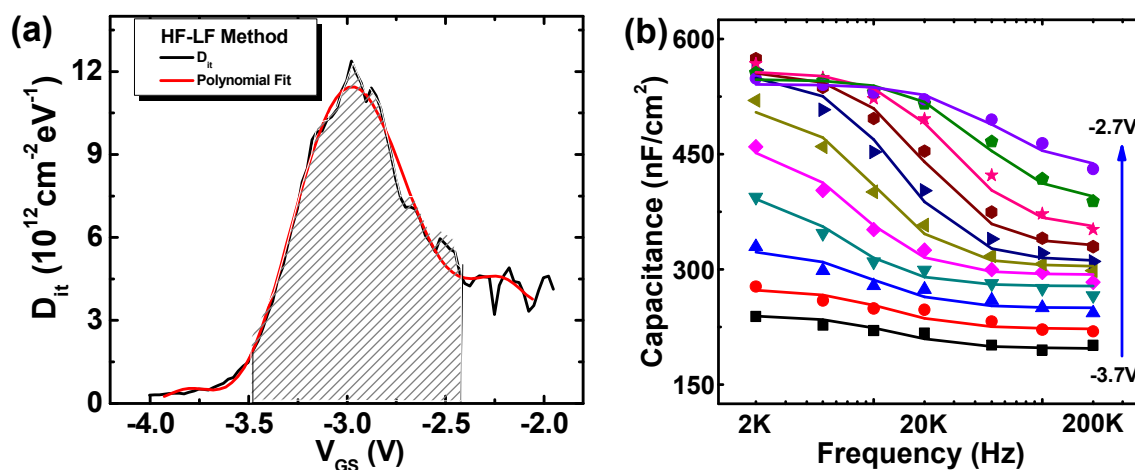
1  
2  
3 In the capacitance-voltage response in the region -4 V to -2 V, a frequency-dependent  
4 distortion (“hump”) in the depletion region is observed, which is consistent with an electrically  
5 activated trap response at the high-*k*/MoS<sub>2</sub> interface region. In conventional Si MOSFETs with  
6 either SiO<sub>2</sub> or high-*k* oxides, this “hump” is usually attributed to interface traps which exhibit a  
7 peak density at a specific energy in the bandgap<sup>36,37</sup>, and usually a forming gas anneal around  
8 400°C can passivate the defects<sup>38,39</sup>, which are primarily silicon dangling bond (P<sub>b</sub>) defects. The  
9 C-V response of Si control sample under the same ALD condition was reported in our previous  
10 work<sup>28</sup>. HfO<sub>2</sub> formed at low temperature (200°C), without any higher temperature annealing in  
11 N<sub>2</sub> or H<sub>2</sub>/N<sub>2</sub> can exhibit gap states which result in C-V hysteresis, interface defect response, and  
12 lower than expected dielectric constant. However, the HfO<sub>2</sub>/Si control sample will not be  
13 representative of the HfO<sub>2</sub>/MoS<sub>2</sub> interface due to the different substrate material and interfacial  
14 condition. (e.g. The Si substrate surface will spontaneously form a SiO<sub>2</sub>-like interfacial layer  
15 during an ALD process, which primarily determines the interfacial property of the HfO<sub>2</sub>/Si<sup>40</sup>).  
16 Published C-V frequency dependence data on a metal / (30nm) HfO<sub>2</sub> / monolayer MoS<sub>2</sub> gate  
17 stack was reported by Zhu et al.<sup>18</sup>, where chemical vapor deposited (CVD) MoS<sub>2</sub> was utilized in  
18 the device structure. Compared with the device based on CVD MoS<sub>2</sub>, this gate stack with  
19 mechanically exfoliated MoS<sub>2</sub> shows much less frequency dispersion, suggesting significantly  
20 fewer interface defects. A limited study of the C-V frequency dependence on semi-bulk MoS<sub>2</sub>  
21 with Al<sub>2</sub>O<sub>3</sub> has also been reported<sup>31</sup>, where interface defects (D<sub>it</sub>) ranging from 10<sup>11</sup> cm<sup>-2</sup>eV<sup>-1</sup> to  
22 10<sup>14</sup> cm<sup>-2</sup>eV<sup>-1</sup> were reported. However, the lateral shift of C-V curves possibly convoluted  
23 positive oxide charge with interface defects in the D<sub>it</sub> extraction process.  
24  
25  
26  
27  
28  
29  
30  
31  
32  
33  
34  
35  
36  
37  
38  
39  
40  
41  
42  
43  
44  
45  
46  
47  
48  
49  
50  
51  
52

53 The techniques that we are about to describe to analyze the D<sub>it</sub> are only valid when the device  
54 is not fully depleted, which must be carefully adhered to when using very thin flakes. In this  
55  
56  
57  
58  
59  
60

1  
2  
3 work, the flake is not fully depleted over the bias range where the  $D_{it}$  response is detected. If the  
4  
5 MoS<sub>2</sub> thin film is fully depleted, the capacitance should be 0 F (or at a constant number over a  
6  
7 voltage range due to parasitic capacitance components)<sup>41</sup>. As shown in Fig. 3a, at about -3V  
8  
9 where interface traps are detected, the transistor is not fully turned off (i.e., not fully depleted and  
10  
11 still has carriers in the flake responding to the AC signal). Further evidence, based on series  
12  
13 resistance analysis (supporting information Fig. S1, S2), confirms that the device is not fully  
14  
15 depleted in the  $V_g$  range used to analyze the  $D_{it}$  from the multi-frequency C-V measurements.  
16  
17 Due to the influence of the interface traps, the inverse subthreshold slope (SS) also increases at  
18  
19 around -3V. This change of SS is also consistent with the charging of MoS<sub>2</sub>/HfO<sub>2</sub> interface traps  
20  
21 providing an independent measurement technique indicating that the C-V response is detecting  
22  
23 interface traps at the corresponding region of the C-V response. SS can be used to roughly  
24  
25 estimate  $D_{it}$  since  $SS = 60\text{mV} \cdot [1 + (C_{dm} + C_{it})/C_{ox}]$ , where  $C_{dm}$  is the capacitance of depleted MoS<sub>2</sub>  
26  
27 and  $C_{it}$  is the capacitance due to interface traps. Thus,  $C_{it}$  and  $D_{it}$  ( $C_{it}/q$ ) can be estimated by  
28  
29 comparing the change in SS around -3.8 V (110 mV/dec) and around -3.2 V (318 mV/dec). The  
30  
31 calculated result gives  $D_{it} = 1.6 \times 10^{13} \text{ cm}^{-2} \text{ eV}^{-1}$ .  
32  
33  
34  
35  
36  
37  
38

39  
40 Next, we quantified the  $D_{it}$  from the C-V response (Fig. 2c). As the frequency is increased  
41  
42 from 1 kHz to 500 kHz, this reduces the AC response of the interface defects to the measured  
43  
44 capacitance, resulting in the dispersion of capacitance with frequency noted in the region from -  
45  
46 2.5 V to -3.5 V in Fig. 2c. In the limit of increasing frequency, the interface defects will only  
47  
48 respond to the DC bias (high frequency  $D_{it}$  response), and the interface states will be evident as a  
49  
50 “plateau” region of the C-V in the case where the interface states are located in a narrow band of  
51  
52 energies. From Fig. 2c, at frequencies above 100 kHz, an approximate plateau region is observed.  
53  
54 At 500 kHz this region extends from -2.8 V and -3.4 V. We interpret this 0.6V gate voltage  
55  
56  
57  
58  
59  
60

region to be due to the DC response of the defects<sup>42</sup>. This is illustrated in schematic energy band diagrams in Fig. 3b, with surface Fermi level pinning due to interface states with a peak density in a specific energy in the band gap<sup>(1)</sup>. The total density of interface defects, in the areal density units of  $\text{cm}^{-2}$ , can be estimated from the oxide capacitance and the width of the plateau region in the 500kHz CV response, and this yields an interface trap density  $D_{it} = 2.7 \times 10^{12} \text{ cm}^{-2}$ . A more detailed calculation is shown in the supporting information S.3. Although the possibility that the defects still respond with AC signal at 500kHz could not be fully excluded, an abrupt C-V distortion due to peaked distribution of interface defects<sup>42</sup> is consistent with our following  $D_{it}$  extraction and analysis.



<sup>(1)</sup> The plateau region is not a constant capacitance. This would only occur for a mono-energetic defect level at a temperature of zero K.

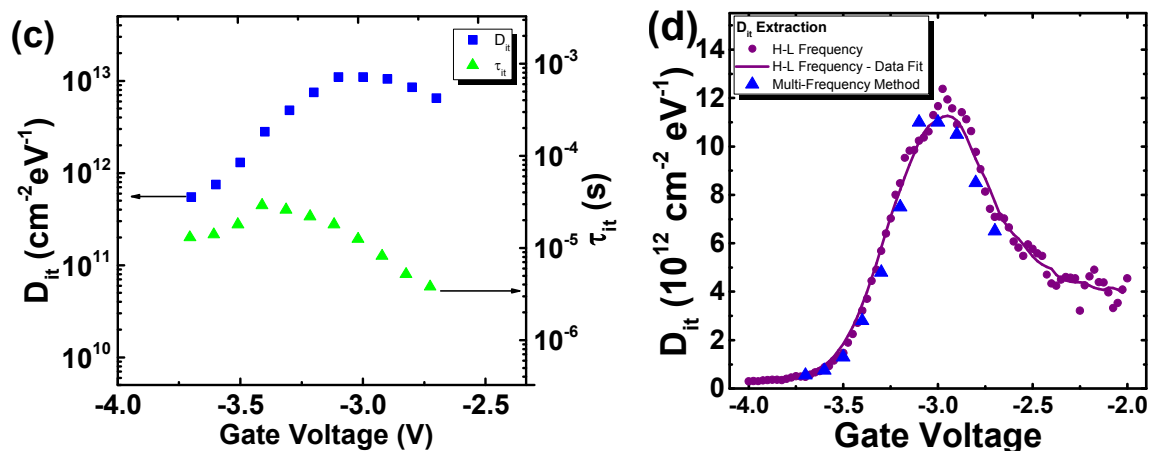


**Figure 4.**  $D_{it}$  extraction. (a)  $D_{it}$  vs  $V_{GS}$ , calculated by High-Low Frequency method; (b) Re-plotted “Capacitance vs Voltage” to “Capacitance vs Frequency” (dots), and modeling (solid lines); (c)  $D_{it}$  vs  $V_{GS}$  and  $\tau_{it}$  vs  $V_{GS}$ , from the modeling work in (b); (d) Comparison of two  $D_{it}$  extraction methods in (a) and (c), showing similar  $D_{it}$  distribution, with a  $D_{it}$  peak at  $1.2 \times 10^{13} \text{ cm}^{-2} \text{eV}^{-1}$ .

Fig. 4a shows the  $D_{it}$  calculated by the conventional high-low frequency method<sup>42</sup> from equations

$$C_{it} = \left( \frac{1}{C_{LF}} - \frac{1}{C_{ox}} \right)^{-1} - \left( \frac{1}{C_{HF}} - \frac{1}{C_{ox}} \right)^{-1} \quad (1)$$

$$D_{it} = C_{it}/q \quad (2)$$

where capacitance of interface traps ( $C_{it}$ ) represents the capacitance when all the traps reacted with AC signal at low frequency;  $C_{LF}$  and  $C_{HF}$  are the capacitance measured at 1 kHz and 500 kHz respectively. In Fig. 4a, the polynomial function is a guide to the eye.  $D_{it}$  ranges from the order of  $10^{12}$  to  $10^{13} \text{ cm}^{-2} \text{eV}^{-1}$ , with a peak value of  $1.2 \times 10^{13} \text{ cm}^{-2} \text{eV}^{-1}$ . The peak value is one order of magnitude lower than what was reported in reference<sup>31</sup> using the same high-low frequency method, and aluminum oxide as the dielectric. It is in the same range as the defect density in literature for exfoliated  $\text{MoS}_2$  by photo-excited charge collection spectroscopy<sup>43</sup>. Translating each gate voltage in Fig. 4a to a corresponding surface potential at the  $\text{MoS}_2/\text{HfO}_2$



1  
2  
3 interface, requires a known value of the active *n*-type doping concentration in the MoS<sub>2</sub>. This  
4  
5 value is not readily known for the geological samples employed here, and as a consequence, the  
6  
7  $D_{it}$  versus energy in the MoS<sub>2</sub> energy gap cannot be determined for these devices.  
8  
9

10  
11 An alternative method was also employed to extract  $D_{it}$ <sup>18</sup>. Instead of only using the C-V data  
12  
13 of high and low frequencies, data from the complete span of frequencies was used, and using this  
14  
15 approach both  $D_{it}$  and the trap time constant  $\tau_{it}$  can be extracted. (The importance of  $\tau_{it}$  is that one  
16  
17 can extract the trap cross section,  $\sigma$ , and trap energy,  $E_T$ , with temperature dependent  
18  
19 experiments<sup>33</sup> to understand the physical origin of the interface traps, and this is beyond the  
20  
21 scope of this work.) In this multi-frequency method,  $C_{it}$  is determined by  $D_{it}$  and  $\tau_{it}$  at certain  
22  
23 voltages.  
24  
25

$$C_{it} = \frac{qD_{it}}{1+\omega^2\tau_{it}^2} \quad (3)$$

26  
27  
28  
29  
30

31 where  $\omega=2\pi f$ , and  $f$  is the applied AC frequency. Thus, at certain voltages,  $D_{it}$  and  $\tau_{it}$  can be  
32  
33 extracted from the C-f or C- $\omega$  relationship. Fig. 4b shows the measured data (symbols) and  
34  
35 model fit (lines) for the capacitance versus frequency for the voltage range corresponding to the  
36  
37 interface defects response in the C-V characteristic. From Fig. 4b, the values of  $D_{it}$ , and the  
38  
39 corresponding  $\tau_{it}$  values, can be determined at each gate voltage, and the characteristics are  
40  
41 shown in Fig. 4c. The two methods are compared in Fig. 4d, demonstrating consistency between  
42  
43 the two  $D_{it}$  extraction approaches. Detailed modeling work for these two methods can be found  
44  
45 in S.3 and S.4.  
46  
47  
48  
49  
50  
51  
52  
53  
54  
55  
56  
57  
58  
59  
60

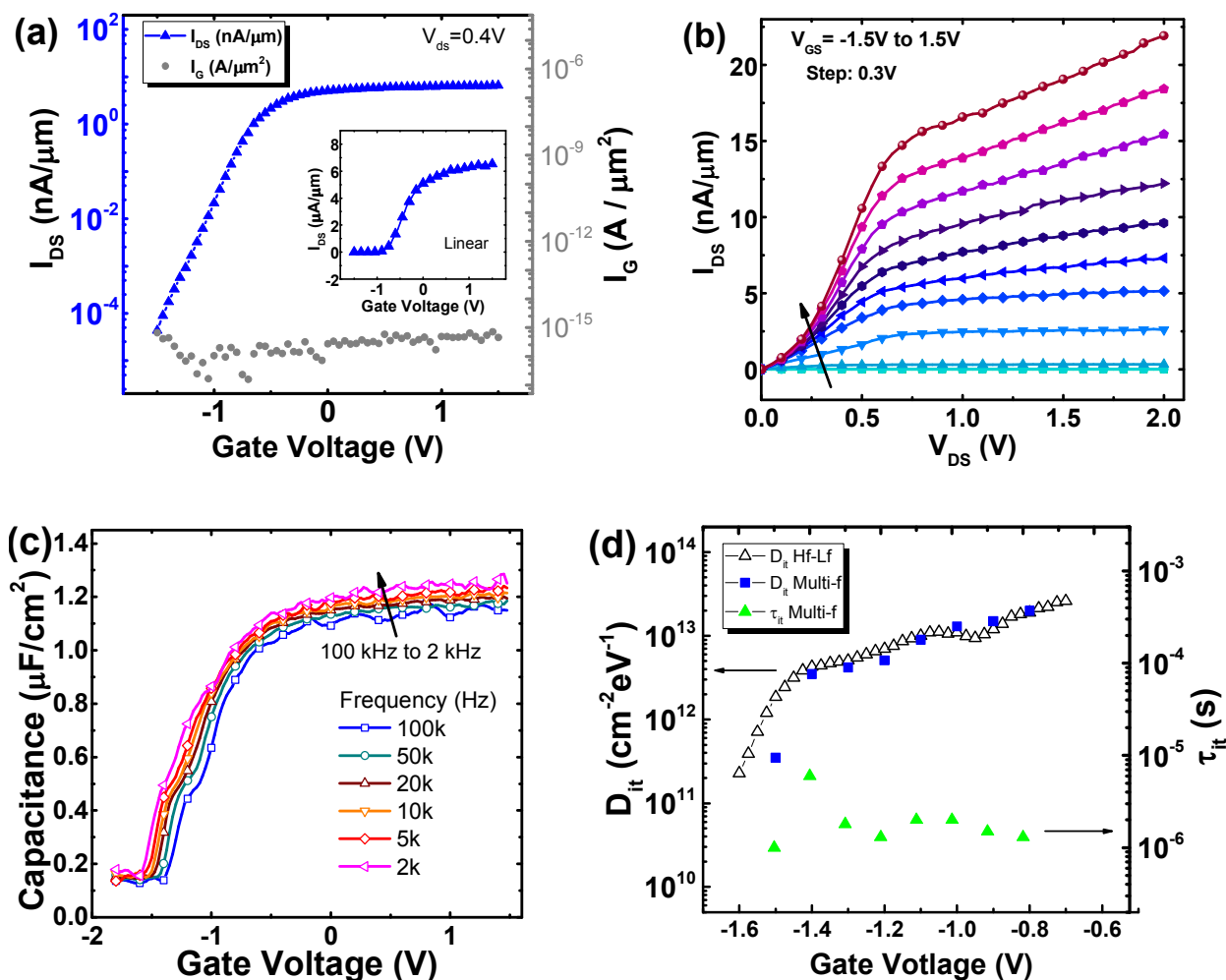


**Figure 5.** Electrical characterization and  $D_{it}$  extraction of a device with 8 nm  $HfO_2$  and 4-layer  $MoS_2$ . ( $W=7.2\mu m$ ,  $L=5.6\mu m$ ) (a)  $I_{DS}$  -  $V_{GS}$  and gate leakage; (b) Corresponding  $I_{DS}$ - $V_{DS}$ ; (c) C-V: frequency dependence; C-V curves disperse in the entire depletion voltage range, indicating interface traps in range of energy levels; (d)  $D_{it}$  vs  $V_{GS}$  and  $\tau_{it}$  vs  $V_{GS}$ ,  $D_{it}$  ranges from  $2 \times 10^{11} cm^{-2} eV^{-1}$  to  $2 \times 10^{13} cm^{-2} eV^{-1}$ , with both H-L frequency method and multi-frequency method.

Due to possible variation in the electronic properties of exfoliated  $MoS_2$  flakes for differing samples, and within a given crystal, in addition to contaminants and the presence of surface defects<sup>44</sup>, we applied the same methods on a different  $MoS_2$  transistor with 8nm  $HfO_2$  and a 4-layer  $MoS_2$  flake to verify if the C-V analysis method is more broadly applicable. Fig. 5a and 5b shows the  $I_{DS}$ - $V_{GS}$ , gate leakage and  $I_{DS}$ - $V_{DS}$  characteristics of this transistor. The gated area is

1  
2  
3 width  $\times$  length = 7.2  $\mu\text{m}$   $\times$  5.6  $\mu\text{m}$ . Fig. 5c and 5d shows the C-V frequency dependence, along  
4  
5 with the extracted  $D_{it}$  with two methods. The C-V frequency dispersion (Fig. 5c) suggests a  
6  
7 different distribution of interface defects at the  $\text{HfO}_2/\text{MoS}_2$  interface compared to the sample  
8  
9 analyzed in Fig. 4. The frequency dependent C-V characteristics are consistent with an interface  
10  
11 state density distributed throughout the  $\text{MoS}_2$  energy gap at the  $\text{HfO}_2/\text{MoS}_2$  interface. Fig. 5d  
12  
13 shows the  $D_{it}$  and  $\tau_{it}$  extracted using high-low frequency and multi-frequency methods. The  
14  
15 magnitude of  $D_{it}$  and  $\tau_{it}$  are comparable to the 7-layer  $\text{MoS}_2$  flake MOSFET shown in Fig. 4, but  
16  
17 in this case no peak in  $D_{it}$  is evident. Similar variation has also been reported in other  
18  
19 publications using thicker  $\text{MoS}_2$  layers<sup>33</sup>, and the variation from sample to sample (with  
20  
21 nominally identical processing) is also manifest in the transport properties<sup>32</sup>. This variability in  
22  
23 interface and transport properties is most likely a consequence of the high density and variability  
24  
25 of impurities and defects in both geological and grown  $\text{MoS}_2$ .<sup>44,45</sup>  
26  
27  
28  
29  
30  
31

32 Interfacial sulfur vacancies<sup>46,47</sup> and other types of surface structural defects<sup>48</sup> are the defects  
33  
34 often observed by researchers, and can potentially generate these defect responses in the  
35  
36 impedance measurement. One possible suggestion for the defect level which shows a peak  
37  
38 response at a specific energy in the band gap (Fig. 4), is that the defect results from sulfur  
39  
40 vacancies<sup>33</sup>, which is reported to have an energy level of 0.35eV from mid gap, from  
41  
42 measurements<sup>46</sup>. The alternative behavior of an almost constant  $D_{it}$  across the energy gap (Fig.  
43  
44 5), observed in this work and in literature<sup>33</sup>, could be a consequence of the area of the certain  
45  
46 devices not containing S vacancies within the gate area probed. Both cases (peaked  $D_{it}$  &  
47  
48 uniform  $D_{it}$ ) were also reported in Ref 33, showing C-V response of MOS capacitors on semi-  
49  
50 bulk  $\text{MoS}_2$  flakes, indicating that the samples that we report in this work are representative. We  
51  
52 also suspect that the defect response observed in our devices can potentially originate from other  
53  
54  
55  
56  
57  
58  
59  
60

1  
2  
3 impurities and defects present in the flake source <sup>44,45</sup> (i.e., the exfoliated MoS<sub>2</sub> crystal), which  
4  
5 can exhibit equivalent surface density values in the range  $1 \times 10^{12}$  to  $1 \times 10^{13}$  cm<sup>-2</sup>. In addition, it is  
6  
7 possible that the response could originate from defects located in an interfacial transition region  
8  
9 between the MoS<sub>2</sub> and the HfO<sub>2</sub> <sup>49–51</sup> because this methodology can also capture border trap  
10  
11 response. This is also the subject of on-going studies.  
12  
13  
14

15  
16 This work provides a relatively easy fabrication procedure and robust electrical  
17  
18 characterization methodology to study top-gated metal / high-*k* / TMD devices. The multi-  
19  
20 frequency C-V response of the structure is consistent with the existence of electrically active  
21  
22 defects at the interface between high-*k* and MoS<sub>2</sub>. By combining with simulation and other  
23  
24 physical characterization, a route to understand and passivate electrically active interface defects  
25  
26 in high-*k* gate TMD MOSFETs is possible .  
27  
28  
29  
30  
31  
32  
33  
34  
35  
36  
37  
38  
39

## 40 **Conclusion**

41  
42  
43 In conclusion, we designed and photolithographically fabricated top-gated FETs on exfoliated,  
44  
45 few-layer MoS<sub>2</sub> flakes, with an in-situ UV-ozone functionalization treatment and 8nm to 13nm  
46  
47 ALD HfO<sub>2</sub> dielectrics. Both the transistor performance and the gate-stack interface properties  
48  
49 were characterized electrically. Based on impedance spectroscopy of the HfO<sub>2</sub>/MoS<sub>2</sub> gate stack  
50  
51 in the MOSFET structure,  $D_{it}$  was extracted from the frequency dependence of the C-V response  
52  
53 using two different methods. The interface state density values were in the range  $1 \times 10^{12}$  to  
54  
55  $1 \times 10^{13}$  cm<sup>-2</sup> eV<sup>-1</sup> for the devices studied, with trapping time constants in the range  $1 \times 10^{-5}$  to  
56  
57  
58  
59  
60

1  
2  
3  $1 \times 10^{-6}$  s. One device with 7-L MoS<sub>2</sub> and 13 nm HfO<sub>2</sub> as the gate oxide exhibited a C-V response  
4  
5 consistent with a D<sub>it</sub> distribution peaking at a value of  $1.2 \times 10^{13}$  cm<sup>-2</sup> eV<sup>-1</sup> at a specific energy in  
6  
7 the MoS<sub>2</sub> band gap. A second device with 4-L MoS<sub>2</sub> and 8 nm HfO<sub>2</sub> yielded D<sub>it</sub> values ranged  
8  
9 from  $2 \times 10^{11}$  cm<sup>-2</sup> eV<sup>-1</sup> to  $2 \times 10^{13}$  cm<sup>-2</sup> eV<sup>-1</sup> with no peak value of D<sub>it</sub> observed. The device  
10  
11 performance and interface properties indicate that the UV-ozone functionalization is promising  
12  
13 for MoS<sub>2</sub>-based devices with high-*k* dielectrics to achieve low leakage, thin and continuous high-  
14  
15 *k* oxide layers, with interface state density values which allow modulation of the Fermi level at  
16  
17 the HfO<sub>2</sub>/MoS<sub>2</sub> interface. The relatively simple MOSFET test structure, combined with the gate  
18  
19 to channel C-V response, indicates the existence of specific electrically active HfO<sub>2</sub>/MoS<sub>2</sub>  
20  
21 interface defects, and combining these results with simulation and other physical  
22  
23 characterization methods, will provide an increased understanding of the physical origin of  
24  
25 defects, as well as a method to monitor the impact of different high-*k* oxides and varying surface  
26  
27 preparations on the interface state density at high-*k*/MoS<sub>2</sub> interfaces.  
28  
29  
30  
31  
32  
33  
34  
35  
36  
37  
38  
39  
40

### 41 **Supporting Information**

42  
43 Proposed equivalent circuits of C-V characterization; Series resistance analysis and full depletion  
44  
45 of MoS<sub>2</sub> flake; Number of interface defects (N<sub>it</sub>) extraction from C-V curves; Defects density  
46  
47 (D<sub>it</sub>) calculation by high-low frequency method; D<sub>it</sub> and traps time constant τ<sub>it</sub> extraction by  
48  
49 multi-frequency method.  
50  
51  
52  
53

### 54 **Corresponding Author**

55  
56  
57 \*E-mail: [chadwin.young@utdallas.edu](mailto:chadwin.young@utdallas.edu)  
58  
59  
60

## Acknowledgment

This work is funded by NSF UNITE US/Ireland R&D Partnership for support under NSF-ECCS-1407765, and Science Foundation Ireland under the US-Ireland R&D Partnership Programme Grant Number SFI/13/US/I2862.

## References

- (1) Wang, Q. H.; Kalantar-Zadeh, K.; Kis, A.; Coleman, J. N.; Strano, M. S. Electronics and Optoelectronics of Two-Dimensional Transition Metal Dichalcogenides. *Nat. Nanotechnol.* **2012**, *7*, 699–712.
- (2) Butler, S. Z.; Hollen, S. M.; Cao, L.; Cui, Y.; Gupta, J. A.; Gutiérrez, H. R.; Heinz, T. F.; Hong, S. S.; Huang, J.; Ismach, A. F.; Johnston-Halperin, E.; Kuno, M.; Plashnitsa, V. V.; Robinson, R. D.; Ruoff, R. S.; Salahuddin, S.; Shan, J.; Shi, L.; Spencer, M. G.; Terrones, M.; Windl, W.; Goldberger, J. E. Progress, Challenges, and Opportunities in Two-Dimensional Materials Beyond Graphene. *ACS Nano* **2013**, *7*, 2898–2926.
- (3) Fiori, G.; Bonaccorso, F.; Iannaccone, G.; Palacios, T.; Neumaier, D.; Seabaugh, A.; Banerjee, S. K.; Colombo, L. Electronics Based on Two-Dimensional Materials. *Nat. Nanotechnol.* **2014**, *9*, 768–779.
- (4) Radisavljevic, B.; Kis, A. Mobility Engineering and a Metal-Insulator Transition in Monolayer MoS<sub>2</sub>. *Nat. Mater.* **2013**, *12*, 815–820.
- (5) Radisavljevic, B.; Radenovic, A.; Brivio, J.; Giacometti, V.; Kis, A. Single-Layer MoS<sub>2</sub> Transistors. *Nat. Nanotechnol.* **2011**, *6*, 147–150.
- (6) Fuhrer, M. S.; Hone, J. Measurement of Mobility in Dual-Gated MoS<sub>2</sub> Transistors. *Nat. Nanotechnol.* **2013**, *8*, 146–147.
- (7) Kaasbjerg, K.; Thygesen, K. S.; Jacobsen, K. W. Phonon-Limited Mobility in N-Type Single-Layer MoS<sub>2</sub> from First Principles. *Phys. Rev. B - Condens. Matter Mater. Phys.* **2012**, *85*, 1–16.

- 1  
2  
3 (8) Das, S.; Chen, H. Y.; Penumatcha, A. V.; Appenzeller, J. High Performance Multilayer MoS<sub>2</sub> Transistors  
4 with Scandium Contacts. *Nano Lett.* **2013**, *13*, 100–105.  
5  
6  
7  
8 (9) Das, S.; Appenzeller, J. Where Does the Current Flow in Two-Dimensional Layered Systems? *Nano Lett.*  
9 **2013**, *13*, 3396–3402.  
10  
11  
12 (10) Kim, S.; Konar, A.; Hwang, W.-S.; Lee, J. H.; Lee, J.; Yang, J.; Jung, C.; Kim, H.; Yoo, J.-B.; Choi, J.-Y.;  
13 Jin, Y. W.; Lee, S. Y.; Jena, D.; Choi, W.; Kim, K. High-Mobility and Low-Power Thin-Film Transistors  
14 Based on Multilayer MoS<sub>2</sub> Crystals. *Nat. Commun.* **2012**, *3*, 1011.  
15  
16  
17 (11) Liu, H.; Ye, P. D. MoS<sub>2</sub> Dual-Gate MOSFET with Atomic-Layer-Deposited Al<sub>2</sub>O<sub>3</sub> as Top-Gate  
18 Dielectric. *IEEE Electron Device Lett.* **2012**, *33*, 546–548.  
19  
20  
21 (12) Ganatra, R.; Zhang, Q. Few-Layer MoS<sub>2</sub>: A Promising Layered Semiconductor. *ACS Nano* **2014**, *8*, 4074–  
22 4099.  
23  
24  
25 (13) Ruppert, C.; Aslan, O. B.; Heinz, T. F. Optical Properties and Band Gap of Single- and Few-Layer MoTe<sub>2</sub>  
26 Crystals. *Nano Lett.* **2014**, *14*, 6231–6236.  
27  
28  
29 (14) Pradhan, N. R.; Rhodes, D.; Feng, S.; Xin, Y.; Memaran, S.; Moon, B. H.; Terrones, H.; Terrones, M.;  
30 Balicas, L. Field-Effect Transistors Based on Few-Layered Alpha-MoTe<sub>2</sub>. *ACS Nano* **2014**, *8*, 5911–5920.  
31  
32  
33 (15) Cui, Y.; Xin, R.; Yu, Z.; Pan, Y.; Ong, Z.; Wei, X.; Wang, J.; Nan, H.; Ni, Z.; Wu, Y.; Chen, T.; Shi, Y.;  
34 Wang, B.; Zhang, G.; Zhang, Y.-W.; Wang, X. High-Performance Monolayer WS<sub>2</sub> Field-Effect Transistors  
35 on High- $\kappa$  Dielectrics. *Adv. Mater.* **2015**, *27*, 5230–5234.  
36  
37  
38 (16) Fang, H.; Chuang, S.; Chang, T. C.; Takei, K.; Takahashi, T.; Javey, A. High-Performance Single Layered  
39 WSe<sub>2</sub> P-FETs with Chemically Doped Contacts. *Nano Lett.* **2012**, *12*, 3788–3792.  
40  
41  
42 (17) Liu, W.; Kang, J.; Sarkar, D.; Khatami, Y.; Jena, D.; Banerjee, K. Role of Metal Contacts in Designing  
43 High-Performance Monolayer N-Type WSe<sub>2</sub> Field Effect Transistors. *Nano Lett.* **2013**, *13*, 1983–1990.  
44  
45  
46 (18) Zhu, W.; Low, T.; Lee, Y.-H.; Wang, H.; Farmer, D. B.; Kong, J.; Xia, F.; Avouris, P. Electronic Transport  
47 and Device Prospects of Monolayer Molybdenum Disulphide Grown by Chemical Vapour Deposition. *Nat.*  
48 *Commun.* **2014**, *5*, 3087.  
49  
50  
51  
52  
53  
54  
55  
56  
57  
58  
59  
60

- 1  
2  
3 (19) Salvatore, G. A.; Münzenrieder, N.; Barraud, C.; Petti, L.; Zysset, C.; Büthe, L.; Ensslin, K.; Tröster, G.  
4  
5 Fabrication and Transfer of Flexible Few-Layers MoS<sub>2</sub> Thin Film Transistors to Any Arbitrary Substrate.  
6  
7 *ACS Nano* **2013**, *7*, 8809–8815.  
8  
9  
10 (20) Jena, D.; Konar, A. Enhancement of Carrier Mobility in Semiconductor Nanostructures by Dielectric  
11  
12 Engineering. *Phys. Rev. Lett.* **2007**, *98*, 1–4.  
13  
14 (21) McDonnell, S.; Brennan, B.; Azcatl, A.; Lu, N.; Dong, H.; Buie, C.; Kim, J.; Hinkle, C. L.; Kim, M. J.;  
15  
16 Wallace, R. M. HfO<sub>2</sub> on MoS<sub>2</sub> by Atomic Layer Deposition: Adsorption Mechanisms and Thickness  
17  
18 Scalability. *ACS Nano* **2013**, *7*, 10354–10361.  
19  
20  
21 (22) Yang, J.; Kim, S.; Choi, W.; Park, S. H.; Jung, Y.; Cho, M.-H.; Kim, H. Improved Growth Behavior of  
22  
23 Atomic-Layer-Deposited High- K Dielectrics on Multilayer MoS<sub>2</sub> by Oxygen Plasma Pretreatment. *ACS*  
24  
25 *Appl. Mater. Interfaces* **2013**, *5*, 4739–4744.  
26  
27  
28 (23) Pezeshki, A.; Hosseini Shokouh, S. H.; Raza, S. R. A.; Kim, J. S.; Min, S.-W.; Shackery, I.; Jun, S. C.; Im, S.  
29  
30 Top and Back Gate Molybdenum Disulfide Transistors Coupled for Logic and Photo-Inverter Operation. *J.*  
31  
32 *Mater. Chem. C* **2014**, *2*, 8023–8028.  
33  
34  
35 (24) Zou, X.; Wang, J.; Chiu, C.-H.; Wu, Y.; Xiao, X.; Jiang, C.; Wu, W.-W.; Mai, L.; Chen, T.; Li, J.; Ho, J. C.;  
36  
37 Liao, L. Interface Engineering for High-Performance Top-Gated MoS<sub>2</sub> Field-Effect Transistors. *Adv. Mater.*  
38  
39 **2014**, *26*, 6255–6261.  
40  
41  
42 (25) Yang, W.; Sun, Q.-Q.; Geng, Y.; Chen, L.; Zhou, P.; Ding, S.-J.; Zhang, D. W. The Integration of Sub-10  
43  
44 Nm Gate Oxide on MoS<sub>2</sub> with Ultra Low Leakage and Enhanced Mobility. *Sci. Rep.* **2015**, *5*, 11921.  
45  
46  
47 (26) Azcatl, A.; McDonnell, S.; K. C., S.; Peng, X.; Dong, H.; Qin, X.; Addou, R.; Mordi, G. I.; Lu, N.; Kim, J.;  
48  
49 Kim, M. J.; Cho, K.; Wallace, R. M. MoS<sub>2</sub> Functionalization for Ultra-Thin Atomic Layer Deposited  
50  
51 Dielectrics. *Appl. Phys. Lett.* **2014**, *104*, 111601.  
52  
53  
54 (27) Azcatl, A.; KC, S.; Peng, X.; Lu, N.; McDonnell, S.; Qin, X.; de Dios, F.; Addou, R.; Kim, J.; Kim, M. J.;  
55  
56 Cho, K.; Wallace, R. M. HfO<sub>2</sub> on UV-O<sub>3</sub> Exposed Transition Metal Dichalcogenides: Interfacial  
57  
58 Reactions Study. *2D Mater.* **2015**, *2*, 14004.  
59  
60

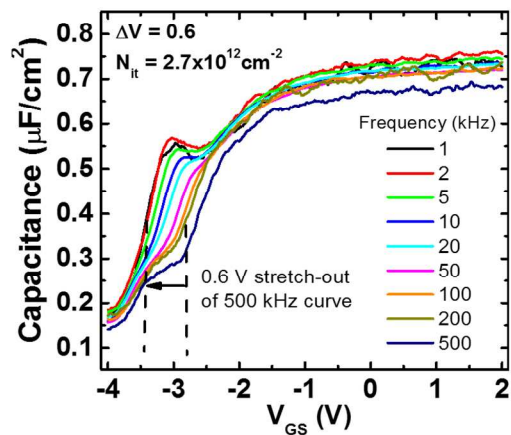
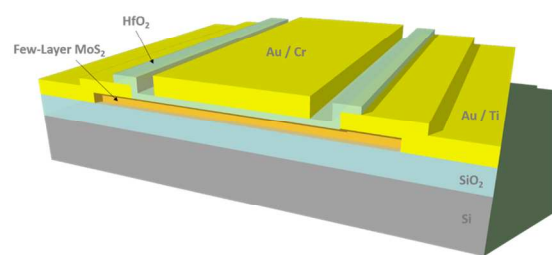
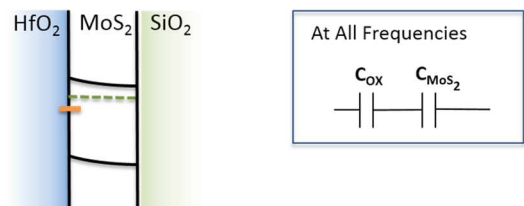


- 1  
2  
3 (28) Zhao, P.; Vyas, P. B.; McDonnell, S.; Bolshakov-Barrett, P.; Azcatl, A.; Hinkle, C. L.; Hurley, P. K.;  
4  
5 Wallace, R. M.; Young, C. D. Electrical Characterization of Top-Gated Molybdenum Disulfide Metal-  
6  
7 oxide-semiconductor Capacitors with High-K Dielectrics. *Microelectron. Eng.* **2015**, *147*, 151–154.  
8  
9  
10 (29) Liu, H.; Si, M.; Deng, Y.; Neal, A. T.; Du, Y.; Najmaei, S.; Ajayan, P. M.; Lou, J.; Ye, P. D. Switching  
11  
12 Mechanism in Single-Layer Molybdenum Disulfide Transistors: An Insight into Current Flow across  
13  
14 Schottky Barriers. *ACS Nano* **2014**, *8*, 1031–1038.  
15  
16 (30) Liu, W.; Sarkar, D.; Kang, J.; Cao, W.; Banerjee, K. Impact of Contact on the Operation and Performance of  
17  
18 Back-Gated Monolayer MoS<sub>2</sub> Field-Effect-Transistors. *ACS Nano* **2015**, *9*, 7904–7912.  
19  
20 (31) Park, S.; Kim, S. Y.; Choi, Y.; Kim, M.; Shin, H.; Kim, J.; Choi, W. Interface Properties of Atomic-Layer-  
21  
22 Deposited Al<sub>2</sub>O<sub>3</sub> Thin Films on Ultraviolet/Ozone-Treated Multilayer MoS<sub>2</sub> Crystals. *ACS Appl. Mater.*  
23  
24 *Interfaces* **2016**, *8*, 11189–11193.  
25  
26 (32) Mori, T.; Ninomiya, N.; Kubo, T.; Uchida, N.; Watanabe, E.; Tsuya, D.; Moriyama, S.; Tanaka, M.; Ando,  
27  
28 A. Characterization of Effective Mobility and Its Degradation Mechanism in MoS<sub>2</sub> MOSFETs. *IEEE Trans.*  
29  
30 *Nanotechnol.* **2016**, *15*, 651–656.  
31  
32 (33) Takenaka, M.; Ozawa, Y.; Han, J.; Takagi, S. Quantitative Evaluation of Energy Distribution of Interface  
33  
34 Trap Density at MoS<sub>2</sub> MOS Interfaces by the Terman Method. *IEEE Int. Electron Devices Meet.* **2016**,  
35  
36 139–142.  
37  
38 (34) Wang, F.; Stepanov, P.; Gray, M.; Ning Lau, C. Annealing and Transport Studies of Suspended  
39  
40 Molybdenum Disulfide Devices. *Nanotechnology* **2015**, *26*, 105709.  
41  
42 (35) Mirabelli, G.; Schmidt, M.; Sheehan, B.; Cherkaoui, K.; Monaghan, S.; Povey, I.; McCarthy, M.; Bell, A. P.;  
43  
44 Nagle, R.; Crupi, F.; Hurley, P. K.; Duffy, R. Back-Gated Nb-Doped MoS<sub>2</sub> Junctionless Field-Effect-  
45  
46 Transistors. *AIP Adv.* **2016**, *6*, 25323.  
47  
48 (36) Cartier, E.; Stathis, J. H. Hot-Electron Induced Passivation of Silicon Dangling Bonds at the Si(111)/SiO<sub>2</sub>  
49  
50 Interface. *Appl. Phys. Lett.* **1996**, *69*, 103.  
51  
52 (37) O’Sullivan, B. J.; Hurley, P. K.; Leveugle, C.; Das, J. H. Si(100)-SiO<sub>2</sub> Interface Properties Following Rapid  
53  
54  
55  
56  
57  
58  
59  
60

- 1  
2  
3 Thermal Processing. *J. Appl. Phys.* **2001**, *89*, 3811–3820.
- 4  
5  
6 (38) Carter, R. J.; Cartier, E.; Kerber, A.; Pantisano, L.; Schram, T.; De Gendt, S.; Heyns, M. Passivation and  
7 Interface State Density of SiO<sub>2</sub>/HfO<sub>2</sub>-Based/polycrystalline-Si Gate Stacks. *Appl. Phys. Lett.*  
8 **2003**, *83*, 533.
- 9  
10  
11  
12 (39) Hurley, P. K.; Cherkaoui, K.; O'Connor, E.; Lemme, M. C.; Gottlob, H. D. B.; Schmidt, M.; Hall, S.; Lu, Y.;  
13 Buiu, O.; Raeissi, B.; Piscator, J.; Engstrom, O.; Newcomb, S. B. Interface Defects in HfO<sub>2</sub>, LaSiO<sub>x</sub>, and  
14 Gd<sub>2</sub>O<sub>3</sub> High-k/Metal–Gate Structures on Silicon. *J. Electrochem. Soc.* **2008**, *155*, G13–G20.
- 15  
16  
17  
18 (40) Bersuker, G.; Park, C. S.; Barnett, J.; Lysaght, P. S.; Kirsch, P. D.; Young, C. D.; Choi, R.; Lee, B. H.;  
19 Foran, B.; van Benthem, K.; Pennycook, S. J.; Lenahan, P. M.; Ryan, J. T. The Effect of Interfacial Layer  
20 Properties on the Performance of Hf-Based Gate Stack Devices. *J. Appl. Phys.* **2006**, *100*, 94108.
- 21  
22  
23 (41) Chen, J.; Solomon, R.; Chan, T.-Y.; Ko, P.-K.; Hu, C. A CV Technique for Measuring Thin SOI Film  
24 Thickness. *IEEE Electron Device Lett.* **1991**, *12*, 453–455.
- 25  
26  
27  
28 (42) Schroder, D. K. *Semiconductor Material and Device Characterization*; John Wiley & Sons, Inc.: Hoboken,  
29 NJ, USA, 2005.
- 30  
31  
32  
33 (43) Choi, K.; Raza, S. R. A.; Lee, H. S.; Jeon, P. J.; Pezeshki, A.; Min, S.-W.; Kim, J. S.; Yoon, W.; Ju, S.-Y.;  
34 Lee, K.; Im, S. Trap Density Probing on Top-Gate MoS<sub>2</sub> Nanosheet Field-Effect Transistors by Photo-  
35 Excited Charge Collection Spectroscopy. *Nanoscale* **2015**, *7*, 5617–5623.
- 36  
37  
38 (44) Addou, R.; McDonnell, S.; Barrera, D.; Guo, Z.; Azcatl, A.; Wang, J.; Zhu, H.; Hinkle, C. L.; Quevedo-  
39 Lopez, M.; Alshareef, H. N.; Colombo, L.; Hsu, J. W. P.; Wallace, R. M. Impurities and Electronic Property  
40 Variations of Natural MoS<sub>2</sub> Crystal Surfaces. *ACS Nano* **2015**, *9*, 9124–9133.
- 41  
42  
43  
44 (45) Addou, R.; Colombo, L.; Wallace, R. M. Surface Defects on Natural MoS<sub>2</sub>. *ACS Appl. Mater. Interfaces*  
45 **2015**, *7*, 11921–11929.
- 46  
47  
48  
49 (46) Qiu, H.; Xu, T.; Wang, Z.; Ren, W.; Nan, H.; Ni, Z.; Chen, Q.; Yuan, S.; Miao, F.; Song, F.; Long, G.; Shi,  
50 Y.; Sun, L.; Wang, J.; Wang, X. Hopping Transport through Defect-Induced Localized States in  
51 Molybdenum Disulphide. *Nat. Commun.* **2013**, *4*, 1–6.
- 52  
53  
54  
55  
56  
57  
58  
59  
60

- 1  
2  
3 (47) Yu, Z.; Pan, Y.; Shen, Y.; Wang, Z.; Ong, Z.-Y.; Xu, T.; Xin, R.; Pan, L.; Wang, B.; Sun, L.; Wang, J.;  
4 Zhang, G.; Zhang, Y. W.; Shi, Y.; Wang, X. Towards Intrinsic Charge Transport in Monolayer  
5 Molybdenum Disulfide by Defect and Interface Engineering. *Nat. Commun.* **2014**, *5*, 5290.  
6  
7  
8  
9  
10 (48) Zhou, W.; Zou, X.; Najmaei, S.; Liu, Z.; Shi, Y.; Kong, J.; Lou, J.; Ajayan, P. M.; Yakobson, B. I.; Idrobo, J.  
11 C. Intrinsic Structural Defects in Monolayer Molybdenum Disulfide. *Nano Lett.* **2013**, *13*, 2615–2622.  
12  
13  
14 (49) Dolui, K.; Rungger, I.; Sanvito, S. Origin of the N-Type and P-Type Conductivity of MoS<sub>2</sub> Monolayers on a  
15 SiO<sub>2</sub> Substrate. *Phys. Rev. B* **2013**, *87*, 165402.  
16  
17  
18  
19 (50) Ghatak, S.; Pal, A. N.; Ghosh, A. Nature of Electronic States in Atomically Thin MoS<sub>2</sub> Field-Effect  
20 Transistors. *ACS Nano* **2011**, *5*, 7707–7712.  
21  
22  
23  
24 (51) Lu, C.-P.; Li, G.; Mao, J.; Wang, L.-M.; Andrei, E. Y. Bandgap, Mid-Gap States, and Gating Effects in MoS  
25 *2. Nano Lett.* **2014**, *14*, 4628–4633.  
26  
27  
28  
29  
30  
31  
32  
33  
34  
35  
36  
37  
38  
39  
40  
41  
42  
43  
44  
45  
46  
47  
48  
49  
50  
51  
52  
53  
54  
55  
56  
57  
58  
59  
60

## Graphic for Table of Contents (TOC)

(i)  $V_{\text{GS}} > -2.8$  V in depletion region(ii)  $-3.4 \text{ V} < V_{\text{GS}} < -2.8$  V ( $E_{\text{F}}$  pinned)